

Digital Predistortion Linearization of a GaN HEMT Push-Pull Power Amplifier for Cable Applications With High Fractional Bandwidth

Pere L. Gilabert¹, Senior Member, IEEE, José-Ramón Pérez-Cisneros², Member, IEEE, Zhixiong Ren, Member, IEEE, Gabriel Montoro, Member, IEEE, María de las Nieves Ruiz Lavín, and José A. García³, Member, IEEE

Abstract—This paper presents two linearization strategies for a custom-designed wideband push-pull (PP) power amplifier (PA) for wired communication applications such as, for example, cable TV. Two digital predistortion (DPD) behavioral models are proposed to meet the in-band and out-of-band linearity requirements when efficiently amplifying wideband DOCSIS signals with high fractional bandwidth (FBW). A radiofrequency (RF) DPD linearizer based on a band-pass generalized memory polynomial (BP-GMP) behavioral model and a baseband (BB) I-Q DPD linearizer based on a harmonic distortion GMP (HD-GMP) behavioral model are proposed. Both DPD models take into account the harmonic distortion typical of high FBW amplification. Experimental results will show high efficient and linear amplification of a 4×192 MHz composite DOCSIS signal by properly combining a crest factor reduction (CFR) technique and the proposed DPD strategies.

Index Terms—Digital predistortion, fractional bandwidth, push-pull power amplifier, power efficiency.

I. INTRODUCTION

IN BOTH wireless and wired environments the need for transmitting signals over long distances makes the power amplifier (PA) one of the key elements in the transmitter side. Not only because it is the main responsible for introducing nonlinear distortion but also because its power consumption is relevant enough to significantly impact capital expenditures (CAPEX) and operational expenditures (OPEX).

In comparison to wireless communications systems, cable distribution systems have their own particularities and consequently, some techniques or solutions used for wireless

systems to deal with the need for high efficient and linear amplification have to be properly adapted. For example, in cable communications the signal spectrum is confined in a cable that is owned and controlled by the operator. In addition, following the data over cable service interface specification (DOCSIS) standard, the signal spans from a few tens or hundreds MHz to about 1.2 GHz. This makes the design and linearization of power efficient PAs very challenging.

From the linearity requirements point of view, in contrast to wireless communications systems, the out-of-band distortion is not a major concern in comparison to the in-band distortion. In order to use high QAM modulation schemes and thus increasing the data throughput, the in-band distortion has to be kept significantly low. In addition, in narrowband wireless systems, only odd distortion products are considered to be contributing to the signal's distortion at the PA output, because the harmonic distortion associated to the even distortion products fall significantly apart from the desired signal bandwidth and thus it can be simply filtered out. In cable applications instead, the fractional bandwidth (FBW) of the transmitted signals is high, which means that even order products fall in-band and contribute to the overall degradation.

Back-off operation is the straightforward solution to guarantee both out-of-band and in-band linearity requirements. However, taking into account that the average power efficiency dramatically drops when the PA is operated far from compression and, considering that the orthogonal frequency division multiplexing (OFDM)-like waveforms of DOCSIS standard present peak-to-average power ratios (PAPRs) greater than 10 dB, back-off operation leads to very low system power efficiencies, typically below 2%.

In order to meet the stringent linearity requirements specified in the DOCSIS standard, digital predistortion linearization (DPD) is the preferred solution due to its potential to compensate for the PA memory effects (impacting the in-band distortion) when considering ultra-wideband signals. For digital terrestrial television applications, for example, Bulusu et al. proposed in [1] a fast convergence DPD based on the memoryless Rapp model. However, only simulations results were provided and thus, the memory effects and fractional bandwidth problems were not properly addressed. There is plenty of literature on digital predistortion (DPD) linearization for wireless cellular communications systems [2], [3], [4], [5].

Manuscript received 6 October 2022; revised 18 January 2023; accepted 3 February 2023. This work was supported in part by the Huawei Technologies and in part by MCIN/AEI/10.13039/50110001103 under Project PID2020-113832RB-C21. (Corresponding author: Pere L. Gilabert.)

Pere L. Gilabert and Gabriel Montoro are with the Department of Signal Theory and Communications, Universitat Politècnica de Catalunya, 08860 Barcelona, Spain (e-mail: plgilabert@tsc.upc.edu).

José-Ramón Pérez-Cisneros was with the Department of Communications Engineering, Universidad de Cantabria, 39005 Santander, Spain. He is now with the Research and Development Department, Ampleon, 31770 Toulouse, France.

Zhixiong Ren is with the Access Network Technology Research Department, Huawei Technologies Company Ltd., Wuhan 430070, China.

María de las Nieves Ruiz Lavín and José A. García are with the Department of Communications Engineering, Universidad de Cantabria, 39005 Santander, Spain.

Digital Object Identifier 10.1109/TBC.2023.3246816

On the contrary, there is few literature addressing the specific linearization problems in cable systems applications. For example, Pratt and Kearney in [6] provide a very accurate description of the main linearization problems (in contrast to wireless cellular communications systems) that need to be faced in cable applications when amplifying wideband signals with high FBW. However, no details on the behavioral models or the DPD adaptation strategy used were detailed in [6] nor in the patent by the same author in [7].

In this paper, for the first time to the best of the author's knowledge, two behavioral models for DPD linearization of cable systems are proposed: one for radiofrequency (RF) DPD and the other for baseband (BB) I-Q DPD. Both models are capable to compensate for the particular in-band and out-of-band nonlinear distortion that appears in signals with high FBW. In addition, a wideband GaN HEMT push-pull PA has been designed with the scope of enhancing power efficiency over a wide bandwidth when operating with significant back-off levels. Finally, the proposed DPD linearization is also properly combined with the peak cancellation (PC) [8] crest factor reduction (CFR) technique to improve the PA power efficiency.

Therefore, the remainder of this paper is organized as follows. Section II begins with a brief explanation of the specific challenges that need to be addressed for the linearization of wideband DOCSIS signals with high FBW. Then, for completeness, follows a description of the PC CFR technique. The main contribution consists in an in depth description of the proposed RF and BB DPD behavioral models, including a description of the greedy algorithm used to properly select the most relevant basis functions of the proposed DPD models. Finally, a detailed explanation of both direct and indirect iterative learning methods used to extract the model coefficients is also provided. Section III presents a description of the design and implementation of the wideband push-pull PA used in this paper as the device-under-test (DUT), as well as the instrumentation-based experimental test bench used to extract results. Experimental results reporting the main characteristics of the designed push-pull PA and the linearization performance of the proposed RF and BB DPD are provided and discussed. Finally, the conclusion is given in Section IV. As it will be proved in the paper, by properly combining CFR and DPD techniques, it is possible to enhance the power efficiency of the push-pull PA when operated with DOCSIS signals expanded over 800 MHz bandwidth while meeting the linearity specifications.

II. DIGITAL SIGNAL PROCESSING TECHNIQUES TO COPE WITH THE PA LINEARITY-EFFICIENCY TRADE-OFF

A. Problem Statement

Digital predistortion linearization has to face several challenges that are particular from cable communication systems, mainly due to the ultra-wideband bandwidth requirements of the signals to be linearized. DPD has to guarantee the required in-band and out-of-band linearity levels in a spectrum that starts only 54 MHz from dc and spans up to around 1.2 GHz. In addition, one of the particular challenges of cable

systems is its FBW, defined as the ratio between the signal bandwidth (BW) and the center frequency of operation f_0 ,

$$\text{FBW} = \frac{\text{BW}}{f_0}. \quad (1)$$

Unlike in wireless system applications where the FBW is significantly smaller than 1 (e.g., in 5G-NR band 7, considering a 40 MHz channel at 2.6 GHz center frequency gives a $\text{FBW} \approx 1.54\%$), in cable systems the FBW is greater than 1 (e.g., 1 GHz BW signal at 700 MHz center frequency gives $\text{FBW} \approx 143\%$). In such high FBW scenario, harmonic distortion (HD) becomes a problem. Unlike in narrowband wireless applications, where HD can be simply removed by filtering because it does not interfere with the signal bandwidth, in wideband cable applications, the HD may fall in-band. Therefore, considering a polynomial behavioral model, the DPD solution has to take into account not only odd order terms (which are enough in narrowband wireless systems to characterize and compensate for the dominant nonlinear distortion) but also even order terms, since these terms will generate nonlinear distortion that will also fall in-band [6].

Fig. 1 shows a simplified block diagram of the baseband subsystems implemented to generate a DOCSIS-like signal and compensate for the nonlinear distortion. DOCSIS-like signals of 192 MHz bandwidth were generated at baseband with a clock rate of 204.8 MSa/s. Then, upsampling is applied to operate at a clock rate of 3.072 GSa/s and channelize the previously generated baseband signals (e.g., in the frequency range from 54 MHz and up to 1.2 GHz). At this point, different digital signal processing compensation strategies have been proposed to deal with the push-pull PA trade-off between power efficiency and linearity. As it will be further detailed in Section II-B, the peak cancellation [8] crest factor reduction technique has been included to be properly combined with DPD and thus try to maximize the power efficiency of the PP PA [9]. In addition, due to the particular characteristics of wired communications, in terms of center frequency of operation and FBW, we have considered and compared two types of DPD linearization approaches:

- RF DPD, where real-valued band-pass signals ($u_{\text{RF}}[n], x_{\text{BB}}[n] \in \mathbb{R}$, see Fig. 1) are used for PA linearization.
- BB I-Q DPD, where complex-valued baseband signals ($u_{\text{BB}}[n], x_{\text{BB}}[n] \in \mathbb{C}$, see Fig. 1) are used PA linearization. In wireless cellular communications scenarios with small FBW, I-Q DPD is the most commonly used solution to cope with the PA nonlinear distortion.

As a device under test (DUT), we designed a push-pull GaN HEMT PA with the scope of enhancing power efficiency over a wide bandwidth when operating with significant back-off levels. As shown in Fig. 1, both BB and RF DPD run at a clock rate of 3.072 GSa/s. Digital upconversion (DUC) and digital downconversion (DDC) to and from the center frequency are included. Further details on the design of the push-pull GaN HEMT PA and the instrumentation used for digital-to-analog and analog-to-digital conversion are given in Section III-A and III-B, respectively.

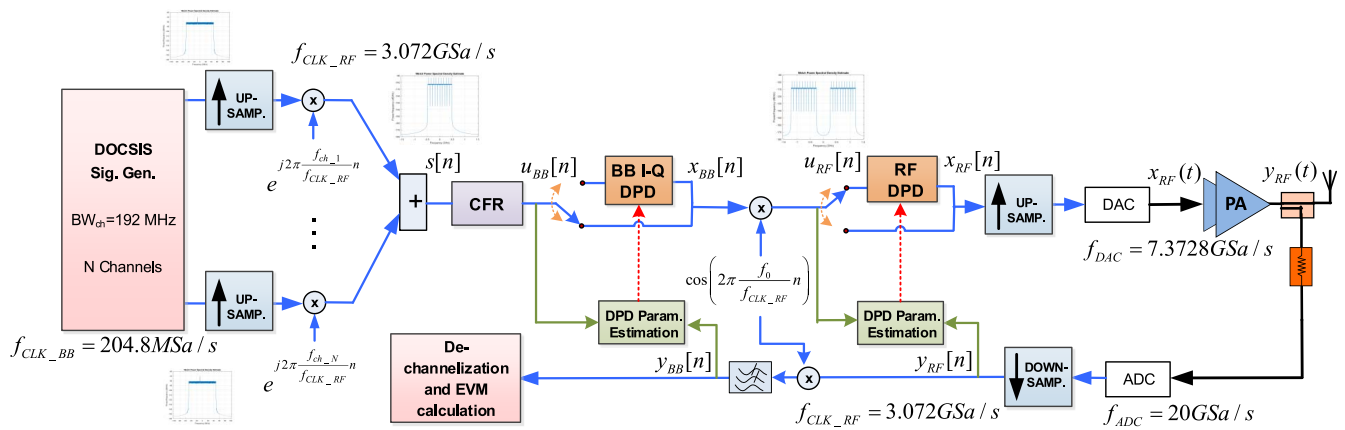


Fig. 1. Simplified block diagram of the digital subsystem including CFR, BB and RF DPD.

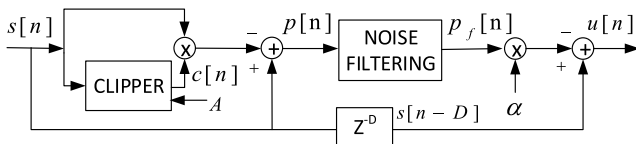


Fig. 2. Block diagram of a peak cancellation cell.

B. Crest Factor Reduction Technique

Among the different CFR techniques proposed in literature to reduce the PAPR of OFDM-based signals [10], [11], [12], we have considered the PC technique, from the family of the clipping and filtering techniques, proposed by Kim et al. in [8]. The main advantages of PC is its reduced computational complexity (in comparison to, for example, CFR techniques that require convex optimization) and that no additional information nor extra signal processing is required at the receiver side. However, the level of PAPR reduction is limited by the amount of in-band distortion that can be tolerated when clipping the signal peaks.

The PC techniques consists in concatenating several CFR cells, depicted in the block diagram of Fig. 2, until reaching the desired PAPR reduction. As shown in Fig. 2, in a first step, a peak signal $p[n]$ is generated as follows,

$$p[n] = s[n] - s[n]c[n] \quad (2)$$

where $s[n]$ is the input signal and $c[n]$ the clipping signal defined as,

$$c[n] = \begin{cases} \frac{A}{|s[n]|} & \text{if } |s[n]| > A \\ 1 & \text{if } |s[n]| \leq A \end{cases} \quad (3)$$

with A being a clipping threshold. In a second step, a filtered or noise-shaped version of the peak signal, $p_f[n]$, is obtained. Finally, the output signal after CFR is calculated by subtracting a weighted version of the filtered peak signal from the original time-aligned input signal,

$$u[n] = s[n - D] - \alpha p_f[n] \quad (4)$$

with α being the subtraction parameter and D the required delay to time-align both signals.

As it will be further discussed in Section III-C, by properly tuning both A and α parameters, it is possible to trade-off the PAPR reduction and the introduction of unwanted in-band distortion.

C. Digital RF DPD

In cable communication applications with high FBW, it is possible to consider the direct synthesis of the RF signal taking into account current commercially available high-speed DACs. For that reason, RF DPD is here proposed as a viable solution to compensate for the PA nonlinear distortion and meet the required in-band and out-of-band linearity specifications.

Volterra series [13] are suitable mathematical descriptors of time-invariant nonlinear systems with fading memory, such as the case of the PA. Considering the RF DPD input-output notation in Fig. 1, the RF DPD output ($x_{RF}[n] \in \mathbb{R}$) taking into account the discrete-time Volterra series formulation is

$$x_{RF}[n] = \sum_{p=1}^P \sum_{q_p=0}^{Q_p-1} \cdots \sum_{q_1=0}^{Q_1-1} h_p(q_1, \dots, q_p) \prod_{i=1}^p u_{RF}[n - q_i]. \quad (5)$$

The parameter P is the number of kernels of the series (the polynomial degree or the order of the nonlinearity), h_p the coefficient associated to the p^{th} kernel and Q_1, \dots, Q_p the memory depths (or number of delays) in each kernel. The main problem of the Volterra series is that the number of coefficients grows significantly when the polynomial degree and memory depth increases. A high-order model may include unnecessary or highly correlated basis functions that may eventually lead to an ill-conditioned least squares (LS) solution.

For PA behavioral modeling and DPD linearization, more simplified polynomial-based behavioral models are usually considered [14]. The RF DPD behavioral model proposed in this paper takes into account cross-memory products as in the generalized memory polynomial (GMP) [15] architecture, but taking into account band-pass signals (i.e., real-valued signals). The RF DPD output of the proposed band-pass GMP

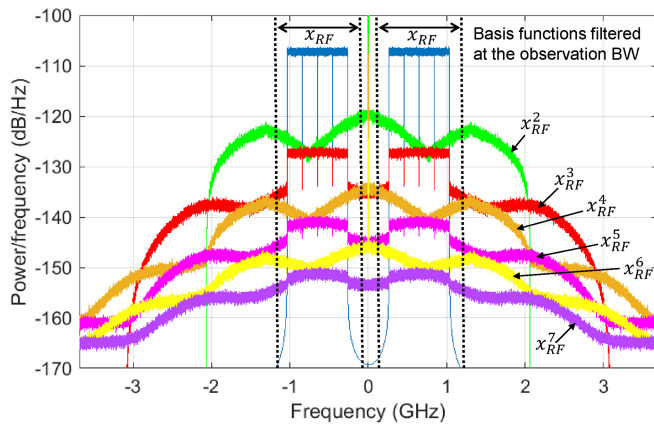


Fig. 3. RF modeling of the spectral regrowth at the PA output taking into account the contribution of different harmonic and intermodulation distortion terms.

(BP-GMP) model is described as follows,

$$x_{RF}[n] = \sum_{p=1}^{P_A} \alpha_p (u_{RF}[n])^p + \sum_{l=0}^{L_B} \sum_{m=0}^{M_B} \sum_{p=0}^{P_B} \beta_{pml} u_{RF}[n - \tau_l^B] (u_{RF}[n - \tau_l^B - \tau_m^B])^p \quad (6)$$

where $u_{RF}[n]$ and $x_{RF}[n]$ are the real-valued RF DPD input and output signals, respectively (see Fig. 1); while P_A and P_B are the polynomial orders. Unlike in narrowband wireless systems, for ultra-wideband cable systems, both even and odd terms are considered. The order P_A of the memoryless polynomial terms in the first branch of (6) is higher than the polynomial order P_B in the second branch, since the second term of (6) is more focused in capturing the PA dynamics (or memory effects) by including nonlinear memory (with cross-memory products) terms. Therefore, L_B and M_B are the number of considered delays and τ_l^B and τ_m^B (with $\tau \in \mathbb{Z}$ and if $\tau_l^B = 0$, then $\tau_m^B \neq 0$) are the most significant sparse delays of the input signal that contribute to characterize memory effects.

Fig. 3 shows the RF modeling of the nonlinear distortion (i.e., spectral regrowth) at the PA output taking into account the contribution of different memoryless harmonic and intermodulation distortion terms. In this case, to model the PA nonlinear behaviour, no DPD is applied and thus $x_{RF} = u_{RF}$. As depicted in Fig. 3, considering a signal composed by 4 channels (each one of 192 MHz bandwidth) with frequency components ranging from 250 MHz to 1050 MHz (i.e., considering a $FBW > 1$), the distortion generated by both even and odd products fall in-band, creating overlapping zones of distortion. This has to be taken later into account to generate the low-pass equivalent behavioral model that will be used for I-Q DPD at baseband.

In order to improve the coefficients identification process and facilitate the re-sampling, we have filtered the basis functions along the observation bandwidth as indicated in Fig. 3. Beyond the observation bandwidth it is not necessary to compensate the signal distortion because we assume that

analog filtering will take care of eliminating the remaining out-of-band distortion.

D. Digital BB DPD

In general, DPD is applied at baseband considering low-pass equivalent behavioral models. In wireless communications, where the FBW is generally low, it is possible to obviate HD and focus only in the intermodulation distortion (IMD) that arises due to the nonlinear behavior of the RF PA. Analogously, the discrete-time low-pass equivalent Volterra series formulation considering complex-valued signals is described as follows,

$$x_{BB}[n] = \sum_{p=1}^P \sum_{q_1=0}^{Q-1} \sum_{q_2=q_1}^{Q-1} \cdots \sum_{q_p=q_{p-1}}^{Q-1} \cdots \sum_{q_{2p-1}=q_{2p-2}}^{Q-1} h_{2p-1}(q_1, q_2, \dots, q_{2p-1}) \prod_{i=1}^p u_{BB}[n - q_i] \prod_{j=p+1}^{2p-1} u_{BB}^*[n - q_j]. \quad (7)$$

where $u_{BB}[n] \in \mathbb{C}$ and $x_{BB}[n] \in \mathbb{C}$ are the BB DPD input and output signals, respectively (see Fig. 1). The series is composed by $2P - 1$ kernels of increasing dimensional order. Again, the main drawback of using the full Volterra series is that the number of parameters grows exponentially when considering higher order kernels. Several alternatives have been proposed in literature to circumvent this problem in wireless communications applications with small FBW.

As depicted in Fig. 3, in applications with high FBW however, such is the case of wideband wired communications for CATV applications, HD can no longer be obviated since it interferes with the signal bandwidth. As an alternative to Volterra series, a low-pass equivalent behavioral model is derived from (6). Following the notation in Fig. 1, the input-output relationship of the proposed HD-GMP parallel behavioral model is described as

$$x_{BB}[n] = \sum_{p=0}^{\frac{P_A-1}{2}} \alpha_p u_{BB}[n] |u_{BB}[n]|^{2p} + \sum_{l=0}^{L_B} \sum_{m=0}^{M_B} \sum_{p=1}^{\frac{P_B}{2}} \beta_{pml} |u_{BB}[n - \tau_l^B]|^p |u_{BB}[n - \tau_l^B - \tau_m^B]|^p \cdot \left(e^{-j\Omega_0 n} + \frac{1}{2} e^{j\Omega_0 n} \right) + \sum_{l=0}^{L_C} \sum_{m=0}^{M_C} \sum_{p=0}^{\frac{P_C-1}{2}} \gamma_{pml} u_{BB}[n - \tau_l^C] |u_{BB}[n - \tau_l^C - \tau_m^C]|^{2p}, \quad (8)$$

where $u_{BB}[n]$ and $x_{BB}[n]$ are the complex-valued baseband DPD input and output signals, respectively. Ω_0 is defined as $\Omega_0 = \frac{2\pi f_0}{f_s}$, with f_0 and f_s being the center and sampling frequencies, respectively. P_A , P_B and P_C determine the nonlinear order of the polynomials at each of the branches of the proposed HD-GMP parallel behavioral model. P_A and P_C have

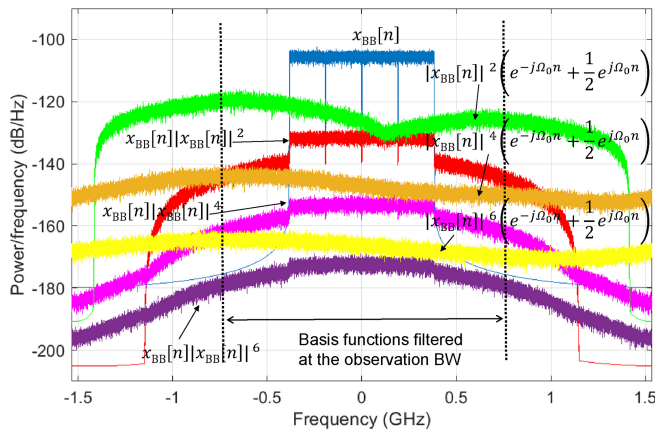


Fig. 4. Baseband modeling of the spectral regrowth at the PA output taking into account the contribution of different harmonic and intermodulation distortion terms.

to be odd numbers, while P_B has to be even. The first branch of the behavioral model in (8) describes the memoryless odd distortion terms, while the third branch describes the odd distortion terms but including memory. M_C and L_C determine the memory depth and τ_I^C and τ_m^C (if $\tau_I^C = 0$, then $\tau_m^C \neq 0$) are the most significant sparse delays. The second branch in (8) instead, describes the even distortion terms (which, again, are of relevance when considering high FBW applications) including memory, where M_B and L_B determine the memory depth and τ_I^B and τ_m^B are the most significant sparse delays. Further details on how to find the most significant basis functions (i.e., parameters configuration) are given in Section II-E.

Fig. 4 shows the baseband modeling of the nonlinear distortion (i.e., spectral regrowth) at the PA output taking into account the contribution of different memoryless harmonic and intermodulation distortion terms. In this case, to model the PA nonlinear behaviour, no DPD is applied and thus $x_{BB} = u_{BB}$. In order to model the HD derived from the even order products, the even order distortion is generated at baseband and then shifted to $-\Omega_0$ and Ω_0 . Similarly to RF DPD, the basis functions are filtered along the observation bandwidth, as indicated in Fig. 4.

E. Selection of the Most Relevant Basis Functions of the DPD Behavioral Models

In order to determine the polynomial orders and the most relevant delays of the proposed DPD behavioral models in (6) and (8), a greedy selection algorithm was considered. The orthogonal matching pursuit (OMP) algorithm can be used to perform an a priori off-line study, to properly select the most relevant basis functions that will contribute to linearize the PA (e.g., [16], [17]). With the OMP, by selecting the most relevant basis, not only the number of required coefficients can be reduced, but also minimizes the risk of having an ill-conditioned system.

To select the most relevant basis contributing to linearize the PA nonlinear behavior, we assume that the optimal subset of selected basis functions of the DPD functions in (6) and (8), will be the same as that used for PA behavioral modeling.

Algorithm 1 Orthogonal Matching Pursuit Algorithm

```

1: procedure OMP ( $y, X$ )
2:   initialization:
3:      $e^{(0)} = y - \hat{y}^{(0)}$ ; with  $\hat{y}^{(0)} = 0$ 
4:      $S^{(0)} = \{\}$ 
5:   for  $m = 1$  to  $m_{max}$  do
6:      $\bar{X}_{\{i\}} \leftarrow \frac{X_{\{i\}}}{\|X_{\{i\}}\|_2}$ 
7:      $i^{(m)} \leftarrow \operatorname{argmax}_i |\bar{X}_{\{i\}}^H e^{(m-1)}|$ 
8:      $S^{(m)} \leftarrow S^{(m-1)} \cup i^{(m)}$ 
9:      $w_{S^{(m)}} \leftarrow (\bar{X}_{S^{(m)}}^H \bar{X}_{S^{(m)}})^{-1} \bar{X}_{S^{(m)}}^H y$ 
10:     $\hat{y}^{(m)} = \bar{X}_{S^{(m)}} w_{S^{(m)}}$ 
11:     $e^{(m)} = y - \hat{y}^{(m)}$ 
12:  end for
13:  return  $S$ 
14: end procedure

```

Therefore, the objective consists on minimizing the number of active components (i.e., ℓ_0 -norm) subject to a constraint on the ℓ_2 -norm squared of the identification error,

$$\begin{aligned} \min_w \quad & \|w\|_0 \\ \text{subject to} \quad & \|y - Xw\|_2^2 \leq \varepsilon. \end{aligned} \quad (9)$$

An approach to address this NP-hard problem, is the use of the OMP greedy algorithm. The OMP search can be conducted off-line, since it relies on input-output observations. The estimated PA behavioral model output $\hat{y}[n]$ (for $n = 0, 1, \dots, L-1$), is defined following a matrix notation as

$$\hat{y} = Xw \quad (10)$$

where $w = (w_1, w_2, \dots, w_M)^T$ is the $M \times 1$ vector of parameters and X is the $L \times M$ data matrix (with $L \gg M$) containing the basis functions or components. The data matrix can be defined as

$$X = \left(\phi_x[0], \phi_x[1], \dots, \phi_x[L-1] \right)^T \quad (11)$$

where $\phi_x^T[n] = (\phi_1^x[n], \phi_2^x[n], \dots, \phi_M^x[n])$ is the $M \times 1$ vector of basis functions $\phi_j^x[n]$ (with $j = 1, \dots, M$) at time n . This general equation can be particularized for any behavioral model, such as the ones proposed in (6) and (8).

For completeness, the OMP algorithm is defined in Algorithm 1. The support set containing the indices of the basis functions describing the PA behavioral model is defined as $S^{(m)}$. Let us consider that m_{max} is the number of basis functions under study, which has to be sufficiently high to ensure a proper exploration. At every iteration of the OMP search, the component (i.e., basis function) that better contributes to minimize the residual error is selected and added to the support set $S^{(m)}$. The index $i^{(m)}$ is obtained by maximizing the absolute value of the dot product between the normalized basis function $\bar{X}_{\{i\}}$ and the residual error $e^{(m-1)}$ of the previous iteration. After a complete OMP search, we obtain a vector $S^{(m_{max})}$ with the indices of all the original basis functions (active components) sorted according to their relevance. Then, by using some information criterion, such as the

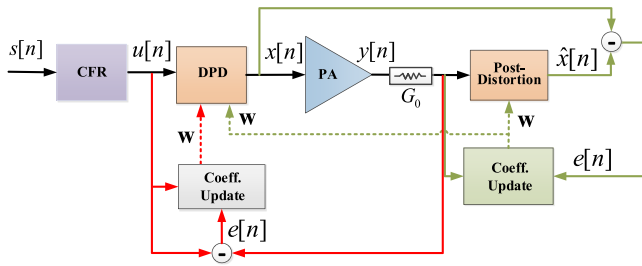


Fig. 5. Block diagram of both direct (red arrows) and indirect (green arrows) learning DPD adaptation.

Akaike (AIC) or the Bayesian (BIC) [16], it is possible to determine the optimum number of coefficients (m_{opt}), where $m_{opt} < m_{max}$. Finally, the subset of selected basis functions, $X_{S(m_{opt})}$, is used in (12) as $U_{S(m_{opt})}$ to carry out the DPD.

F. Adaptive DPD Identification

Fig. 5 shows the block diagram of the adaptive DPD subsystem for both direct and indirect learning modes. This general block diagram is valid for both BB and RF adaptation approaches. For simplicity, in the following the DPD adaptation will be described using the notation for baseband DPD.

In the forward path, the input-output relationship in the DPD block can be defined following the notation in Fig. 5 as,

$$\mathbf{x} = \mathbf{u} - \mathbf{U}\mathbf{w} \quad (12)$$

where \mathbf{u} is the $L \times 1$ input vector and L is the number of samples (i.e., $n = 0, 1, L-1$), \mathbf{x} is the $L \times 1$ predistorted vector and \mathbf{w} is the $M \times 1$ vector of coefficients. The $L \times M$ data matrix \mathbf{U} containing the basis functions is defined as

$$\mathbf{U} = \left(\phi_u[0], \phi_u[1], \dots, \phi_u[L-1] \right)^T \quad (13)$$

where $\phi_u[n]$ is the $M \times 1$ vector of basis functions $\phi_j^u[n]$, for $j = 1, \dots, M$, at time n .

$$\phi_u^T[n] = \left(\phi_1^u[n], \phi_2^u[n], \dots, \phi_M^u[n] \right) \quad (14)$$

These basis functions can be particularized taking into account any behavioral model. In this paper, we have employed the basis functions from both the BP-GMP behavioral model in (6) for RF DPD and the HD-GMP behavioral model in (8) for BB I-Q DPD.

Applying an iterative learning approach, the DPD coefficients at the k^{th} iteration can be calculated as follows,

$$\mathbf{w}^{k+1} = \mathbf{w}^k + \mu \Delta \mathbf{w}. \quad (15)$$

with μ ($0 < \mu < 1$) being a learning rate parameter. Now, following a direct learning (DL) approach as proposed in [18], [19], the least squares (LS) solution for $\Delta \mathbf{w}$ is defined as

$$\Delta \mathbf{w} = (\mathbf{U}^H \mathbf{U})^{-1} \mathbf{U}^H \mathbf{e}_{DL} \quad (16)$$

with \mathbf{e}_{DL} being the $L \times 1$ vector of the DL residual error, defined as

$$\mathbf{e}_{DL} = \frac{\mathbf{y}}{G_0} - \mathbf{u} \quad (17)$$

where the desired linear gain is G_0 .

Unlike the direct learning approach, in the indirect learning (IL) approach we first estimate the inverse PA model by postdistorting the PA output signal. This is based on the assumption that the coefficients of the postdistorter and the coefficients of the predistorter are equivalent. As depicted in Fig. 5, the output of postdistorter is defined as

$$\hat{\mathbf{x}} = \frac{\mathbf{y}}{G_0} - \mathbf{Y}\mathbf{w} \quad (18)$$

where \mathbf{y} is the $L \times 1$ PA output vector (i.e., the postdistorter input). Analogously, the $L \times M$ data matrix \mathbf{Y} , containing the basis functions, is calculated as \mathbf{U} in (13)-(14), but using signal $\frac{\mathbf{y}}{G_0}$ instead of signal \mathbf{u} ,

$$\mathbf{Y} = \left(\phi_y[0], \phi_y[1], \dots, \phi_y[L-1] \right)^T \quad (19)$$

where $\phi_y[n]$ is the $M \times 1$ vector of basis functions $\phi_j^y[n]$, for $j = 1, \dots, M$, at time n .

$$\phi_y^T[n] = \left(\phi_1^y[n], \phi_2^y[n], \dots, \phi_M^y[n] \right) \quad (20)$$

where again, in general, the basis functions can be particularized taking into account any of the existing behavioral models.

The new vector of postdistorter coefficients \mathbf{w} is updated at the k^{th} iteration as in (15), where the LS solution for $\Delta \mathbf{w}$ considering the IL approach is defined as

$$\Delta \mathbf{w} = (\mathbf{Y}^H \mathbf{Y})^{-1} \mathbf{Y}^H \mathbf{e}_{IL} \quad (21)$$

The $L \times 1$ IL postdistortion estimation error vector \mathbf{e}_{IL} is defined as

$$\mathbf{e}_{IL} = \mathbf{x} - \hat{\mathbf{x}}. \quad (22)$$

As depicted in Fig. 5, once the postdistortion coefficients \mathbf{w} are estimated, they are copied and used in the DPD subsystem in the forward path, as described in (12).

III. POWER AMPLIFIER, EXPERIMENTAL TEST-BENCH AND RESULTS

A. Power Amplifier Design

A wideband PA using GaN HEMT technology was designed and implemented to produce competitive power efficiency values in comparison to the commercial cable television (CATV) parts currently under use. Fig. 6 shows both the schematic and the table of components of the designed amplifier. A push-pull architecture was chosen for exploiting its intrinsic rejection to even-order distortion components.

The size and drain biasing voltage range of the employed GaN HEMT devices were selected to place their high efficiency load-pull contours in a region over the Smith Chart that could facilitate synthesizing the desired drain impedance at the fundamental over a wide frequency range. The gate biasing voltage was adjusted slightly above the pinch-off value of the process ($V_p = -2.8$ V) as a compromise between predistortion gain and phase profiles and a reduced degradation of efficiency under output power back-off (OBO) condition. A small-valued coil was selected for the drain biasing path in order to reduce its possible contribution to memory effects.

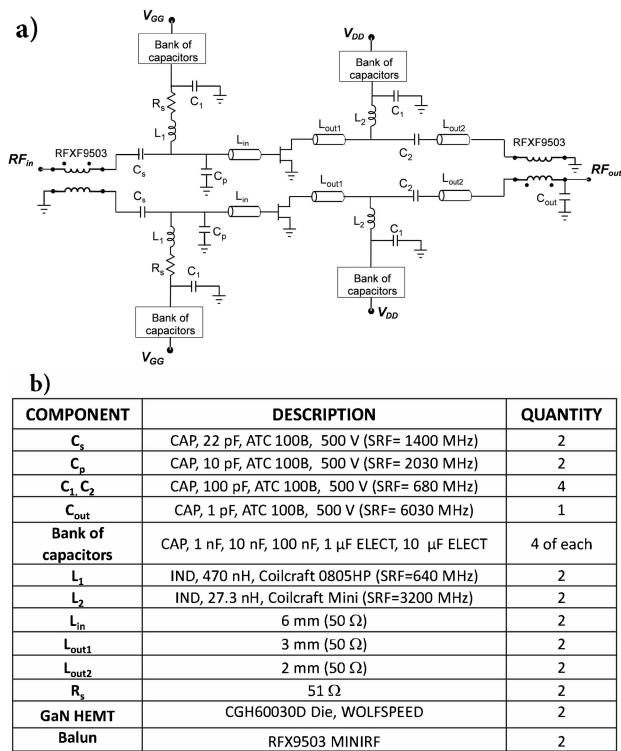


Fig. 6. a) Schematic and b) table of components of die-based Push-pull PA.

Fig. 7-a) shows a photograph of the implemented lab prototype. Advantage was taken of components with reduced footprints. Commercial baluns (MiniRF) and die-based GaN HEMTs (Wolfsped) were combined with high-Q capacitors from ATC (100 A Series) and inductors from Coilcraft (Square Air Core and Ceramic Core Chip Series). The banks of capacitors were placed close to the biasing connectors. Due to the size of the Aluminium carrier used for the implementation, the power density potential of the topology was not fully exploited. In Fig. 7-b), an optimized layout is presented, showing the active region area of the amplifier could be easily reduced below 38mm \times 30mm.

Simulation results in Fig. 8 show the power gain and efficiency evolution with output power at different frequency values for a continuous wave (CW) excitation. Flat gain profiles above 20 dB may be observed, with a variation below 3 dB across such a wide frequency range for small-signal operation, followed by the expected deep compression when the output power saturates. The maximum efficiency reaches 69.2% at the central frequency of 700 MHz, for a peak output power of 41.3 dBm, staying above 60% from 200 MHz up to 1100 MHz. Under a deep OBO value of 12 dB, the efficiency remains above 7% for most part of the band to be covered, reaching 9% at the central frequency.

B. Experimental Test-Bench

The designed wideband push-pull PA described in the previous subsection, was experimentally evaluated with DOCSIS signals using a MATLAB-controlled test bench that interfaces waveform generation and acquisition instruments,

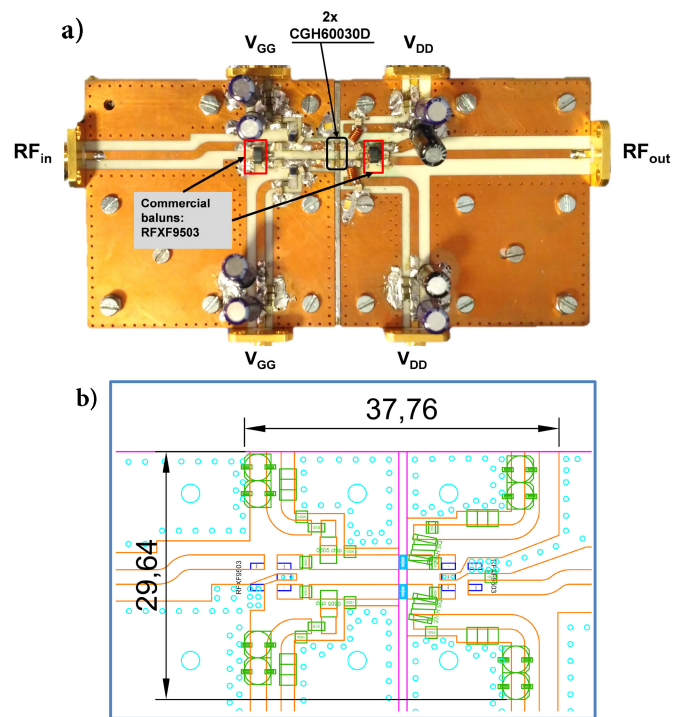


Fig. 7. a) Photograph and b) layout size detail in mm of die-based Push-pull PA.

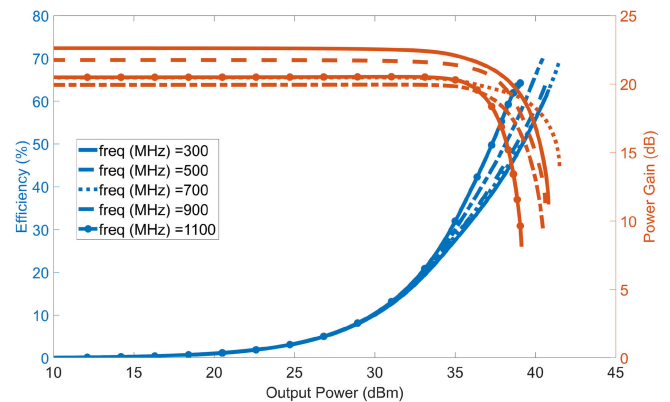


Fig. 8. Power gain and efficiency profiles versus output power from simulations (CW excitation).

as shown in Fig. 9-a). In order facilitate the remote collaboration between the research group located and the Universitat Politècnica de Catalunya (UPC) and the research group located at the Universidad de Cantabria (UC), a MATLAB client-server waveform upload/download architecture was enabled. This setup permitted launching multiple DPD experiments in parallel and from different physical locations. The MATLAB server communicated both with the remote clients running the DPD algorithms and the laboratory hardware located at the UC.

The direct RF generation at $f_0=650$ MHz of approximately 800 MHz bandwidth (4 channels \times 192 MHz BW, ranging from 250 MHz and up to 1050 MHz) of 64 QAM (OFDM-based) DOCSIS signals with a PAPR of around 11 dB, was carried out through the arbitrary waveform generator AWG

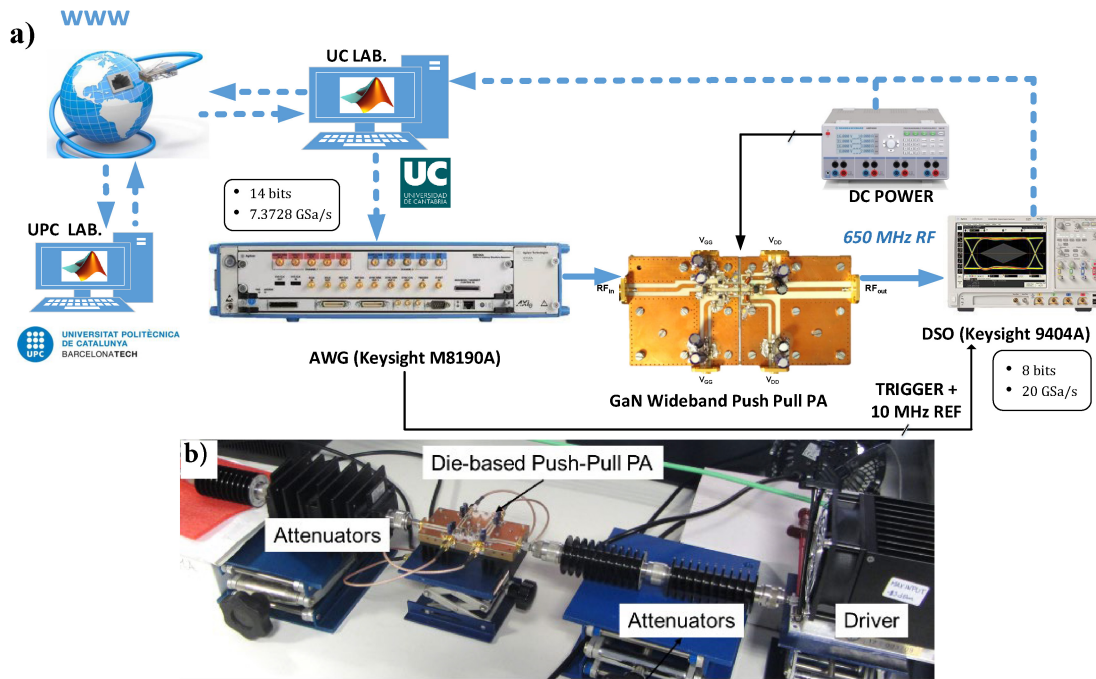


Fig. 9. a) Block diagram and b) photograph of the experimental test bench.

M8190A from Keysight, with a clock rate of 7.3728 GSa/s and 14 bits. A digital storage oscilloscope (Keysight 9404A) was used to acquire the RF output signal at 20 GSa/s with 8-bit resolution. Averaging was required to improve the SNR of the acquired signal (noise level around -50 dB approximately).

As depicted in Fig. 9-b), an attenuator was included at the input of the PP PA to avoid any undesired interaction, considering the PA input matching and the driver output matching could not be the best across the complete frequency range. The employed pre-amplifier was the Minicircuits ZHL-20W-13+, which may offer up to 41 dBm from 20 to 1100 MHz, allowing enough margin to drive the DUT with the aforementioned attenuation. Recommended for operation up to 1000 MHz, its output VSWR is above 2 for a significant part this range, with values even higher than 3 at some frequencies. Since its gain versus frequency profile falls down 5 dB at 1200 MHz, a reduced bandwidth signal (4 channels, 300 to 1100 MHz) was selected for the dynamic tests.

After a first characterization of the implemented PA shown in Fig. 7-a), the input and output matching/terminating networks were readjusted in order to obtain a response as flat as possible (≈ 15 dB, as shown in Fig. 10-a)) for the small signal gain and in order to increase the efficiency at higher frequencies, respectively. Due to the limited power handling capability of the employed baluns, a CW large-signal characterization of the PA was prohibitive. As alternative, a pulsed RF excitation was employed with a duty cycle of 5% and a pulse width of 50 μ sec.

As depicted in Fig. 10-b), a saturated output power higher than 40 dBm was measured from 200 to 1200 MHz. The drain efficiency remains above 56.5% for the whole frequency band (above 60% from 210 to 1150 MHz). A peak value higher than 70% was also measured. The PAE is above 55% from 210 to 1130 MHz, for a 920 MHz frequency span.

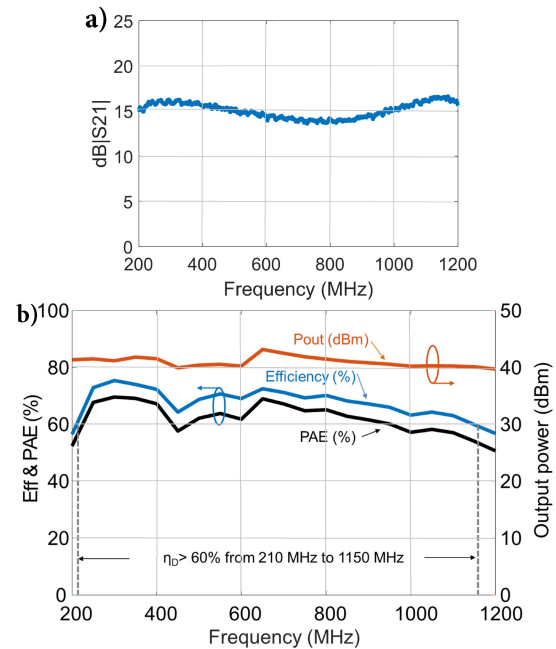


Fig. 10. a) Small-signal gain together with b) efficiency, PAE and output power profiles at saturation under pulsed RF excitation.

C. Experimental Results on DPD Linearization

Taking into account that the RF signal is band-pass filtered after the RF PA, we assume that the out-of-band distortion compensation has to be carried out up to a certain observation bandwidth only. Consequently, in order to quantify the out-of-band distortion compensation, the adjacent channel power ratio (ACPR) was measured considering a 100 MHz offset (this offset should be reduced to 50 MHz when the lower signal frequency is 54 MHz) from the lowest and highest frequency

TABLE I
COMPARISON OF WIDEBAND DPD LINEARIZATION STRATEGIES WITH
PUSH-PULL PA POLARIZATION $V_{GG} = -2.6\text{V}$, $V_{DD} = 16\text{V}$

DPD config.	num. coeff.	ACPR (dBc)	EVM (dB)	P_{out} (dBm)	η (%)
#0) NO DPD (PAPR=11.1 dB)	0	-25.1/-22.6	-31.9	29.6	8.9
#1) NO DPD (Back-off)	0	-36.2/-36.4	-43.8	25.3	3.1
#2) I-Q DPD (PAPR=11.1 dB)	387	-41.3/-40.3	-46.0	24.6	2.6
#3) I-Q DPD (PAPR=11.1 dB)	387	-40.9/-39.3	-46.2	25.2	3.0
#4) RF DPD (PAPR=11.1 dB)	391	-40.6/-42.8	-46.6	25.4	3.2
#5) RF DPD+CFR (PAPR=9 dB)	391	-40.7/-42.5	-44.7	26.0	3.7

components. Beyond the lower and upper 100 MHz offset, the signal is filtered and the ACPR values are more easily met. As previously discussed, in wired communications systems, the out-of-band distortion is not a major concern in comparison to the in-band distortion requirements, where stringent error vector magnitude (EVM) figures have to be met in order to employ high QAM modulation schemes (that allow increasing the data throughput).

Both BB and RF DPD run at a clock rate of 3.072 GSa/s. Therefore, all basis functions are generated at 3.072 GSa/s and then filtered along an observation bandwidth of 1 GHz. We are assuming that some frequency wrapping occurs when considering basis functions with high order nonlinear terms. However, these unwanted effects occur mainly at high frequencies (i.e., around $f_s/2 = 1.536\text{ GHz}$). Thus, since the observation bandwidth for filtering is set to 1 GHz, the unwanted effects due to aliasing are considered to be negligible. The reason to assume this slight degradation (but yet meeting the linearity specifications) is to avoid the additional computational complexity of up-sampling, filtering and down-sampling that would be necessary to generate each nonlinear basis function (i.e., for each nonlinear basis function, f_s should be $P \times BW$, where P is the nonlinear order).

In a first approach, we compared the linearization performance of the proposed RF DPD linearizer based on a BP-GMP behavioral model and the BB I-Q DPD linearizer based on a HD-GMP behavioral model, in terms of ACPR and EVM. As shown in Table I, the targeted linearization specifications of $ACPR \leq -40\text{ dBc}$ and $EVM \leq -45\text{ dB}$ were met with both RF and I-Q DPD when considering a PA polarization of $V_{GG} = -2.6\text{ V}$ and $V_{DD} = 16\text{ V}$. By controlling the output back-off, it is possible to improve the out-of-band distortion compensation (measured in terms of ACPR) at the price of having lower output power and thus power efficiency. This effect can be observed either without DPD (e.g., configuration #0 versus configuration #1 in Table I), or after applying DPD (e.g., configuration #2 versus configuration #3 in Table I). In addition, Fig. 11, Fig. 12, Fig. 13 and Fig. 14 show the unlinearized and linearized output power spectra, the AM-AM and AM-PM characteristics when considering I-Q DPD with no CFR (i.e., configuration #2 in Table I) and RF

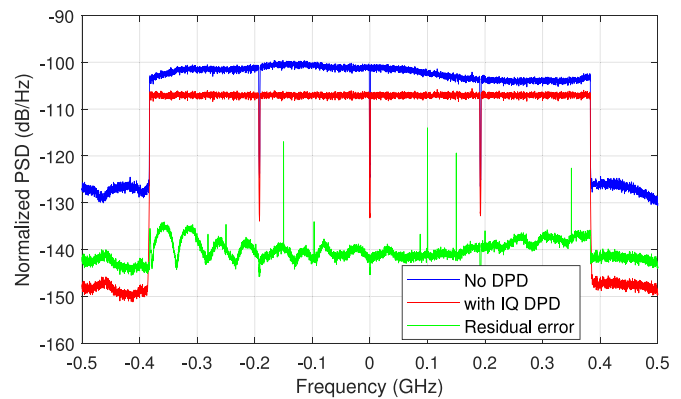


Fig. 11. Unlinearized and linearized (configurations #0 and #2, respectively, in Table I) PP PA output spectra when considering BB IQ DPD without CFR.

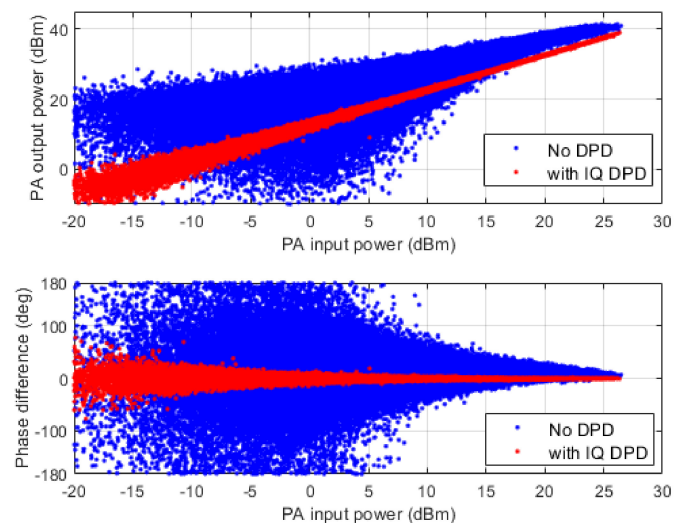


Fig. 12. AM-AM and AM-PM characteristics without and with BB IQ DPD and no CFR (configurations #0 and #2, respectively, in Table I).

DPD with CFR (i.e., configuration #5 in Table I), respectively. As observed, slightly better out-of-band distortion compensation in the upper band can be achieved using RF DPD. In addition, in order to maximize the power efficiency, PC CFR is applied and thus, as reported in Table I, it is possible to slightly increase the mean output power and, consequently, the PA power efficiency. On the contrary, if no CFR is considered (see for example Fig. 11 and Fig. 12) we have to operate with higher back-off to meet the linearity specifications, which impacts the power efficiency (as reported in Table I). The price to pay when reducing the PAPR by using CFR techniques is a degradation of the EVM, since additional in-band distortion is introduced by using the PC CFR technique.

As, described in Section II-E, in order to select the most relevant DPD basis functions we used the OMP algorithm. Taking into account the BP-GMP behavioral model described in (6), the number of parameters of this model can be calculated as follows: $M = P_A + (P_B + 1)(L_B M_B - 1)$. For the OMP search, the initial configuration of the hyper-parameters of the BP-GMP model was: $P_A = 13$, $P_B = 5$, $L_B = 51$ with $\tau_l^B = [0 : 50]$ and $M_B = 5$ with $\tau_m^B = [-2 : 2]$, except for

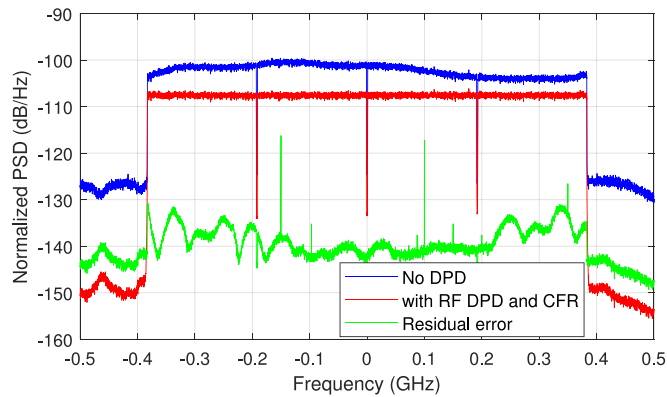


Fig. 13. Unlinearized and linearized (configurations #0 and #5, respectively, in Table I) PP PA output spectra when considering RF DPD with PC CFR.

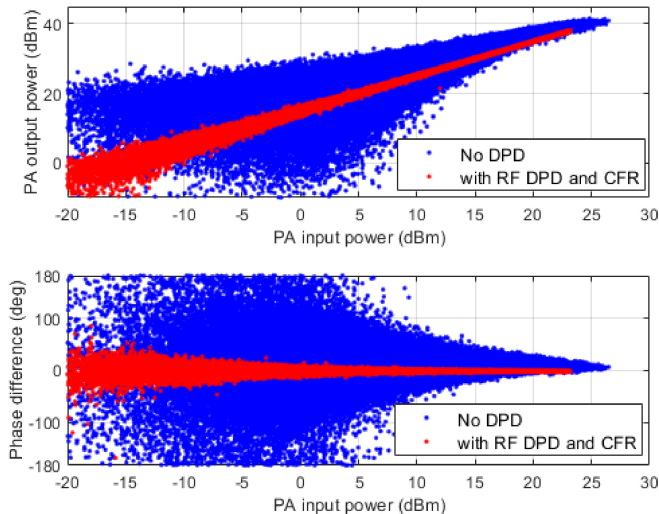


Fig. 14. AM-AM and AM-PM characteristics without and with RF DPD and PC CFR (configurations #0 and #5, respectively, in Table I).

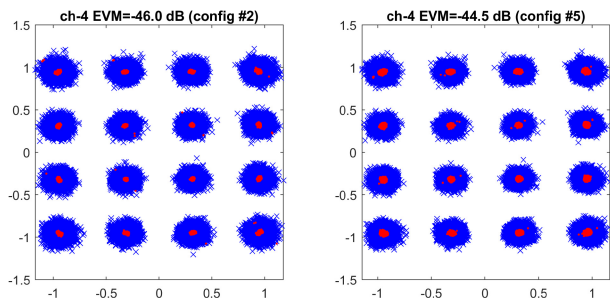


Fig. 15. Constellation of channel 4 (worst-case), without DPD (blue) and with IQ DPD and No CFR (red, left-figure) and with RF DPD and CFR (red, right-figure), corresponding to configurations #0, #2 and #5 in Table I, respectively.

the case of $\tau_l^B = 0$ and $\tau_m^B = 0$. Therefore, the initial configuration consisted of $m_{max} = 1537$ coefficients in Algorithm 1. After the OMP search, the number of coefficients was reduced to $m_{opt} = 391$. Analogously, the number of parameters of the HD-GMP parallel behavioral model described in (8), can be calculated as follows: $M = (\frac{P_A+1}{2}) + (\frac{P_B}{2})L_B M_B + (\frac{P_C+1}{2})(L_C M_C - 1)$. For the OMP search, the initial configuration of the hyper-parameters of the HD-GMP behavioral

TABLE II
COMPARISON OF PA POLARIZATION STRATEGIES COMBINED WITH CFR (ORIGINAL PAPR=11.1 dB) AND DPD LINEARIZATION (ACPR \leq -40 dBc EVM \leq -45 dB)

PP PA polarization	PAPR (dB) with CFR	P _{out} (dBm)	η (%)
$V_{GG}=-2.6$ V; $V_{DD}=16$ V	9.0	26.0	3.7
$V_{GG}=-2.5$ V; $V_{DD}=10$ V	10.0	26.9	6.1
$V_{GG}=-2.45$ V; $V_{DD}=8.5$ V	9.5	27.3	7.3

model was: $P_A = 13$, $P_B = 6$, $P_C = 5$, $L_B = 51$ with $\tau_l^B = [0 : 50]$, $M_B = 5$ with $\tau_m^B = [-2 : 2]$, $L_C = 51$ with $\tau_l^C = [0 : 50]$, $M_C = 5$ with $\tau_m^C = [-2 : 2]$, except for the case of $\tau_l^C = 0$ and $\tau_m^C = 0$. Therefore, the initial configuration consisted of $m_{max} = 1534$ coefficients in Algorithm 1. After the OMP search, the number of coefficients were reduced to $m_{opt} = 387$.

Despite the fact that the number of DPD coefficients (slightly less than 400 coefficients) in both RF and DPD cases may look high when comparing it to DPD solutions for narrowband signal in wireless systems, it is the minimum number of required DPD coefficients to meet both in-band and out-of-band linearity specifications when considering a wide-band signal and high FBW. We indistinctly estimated the DPD coefficients adaptively using both direct and indirect learning approaches. While the indirect learning approach shows faster convergence (in around 3 iterations), the direct learning approach can achieve better in-band linearization figures (around 1 dB better) after 8 iterations. In both cases, the learning rate parameter μ in (15), was initially set to 0.99 and then decreased 0.1 at every iteration up to a minimum of value of 0.2, to guarantee a smooth convergence.

Although in a first approach the drain biasing voltage value of 16 V was selected for the GaN HEMTs in the power amplifier, the obtained results after applying the DPD with CFR showed there was some margin left to better adjust the power capability of the push-pull PA to the DOCSIS signals. Table II shows the output power values and power efficiency figures for different configurations of the gate and drain voltages when CFR and DPD were applied to help meeting the specifications of ACPR of -40 dBc and EVM of -45 dB. By reducing V_{DD} and slightly increasing V_{GG} , the gain and efficiency profiles follow a similar behavior as those reported in Fig. 8, but with enhanced peak efficiency values. That is the reason why both biasing voltages were tuned in order to find a more efficient configuration while meeting the linearity specifications.

As explained before, when combining CFR with DPD the power efficiency can be improved at the price of degrading the in-band linearity (i.e., the EVM). Fig. 16 shows the power efficiency and the best EVM (out of 4 channels) for different PAPR values when considering the PA polarization of $V_{GG} = -2.45$ V and $V_{DD} = 8.5$ V. As observed, even without the PA, the EVM is degraded due to the clipping and filtering nature of the PC technique. In the absence of noise and other residual distortion due to the RF PA, a PAPR reduction of around 2.6 dB can be achieved and still being compliant the -45 dB specifications of EVM. The ACLR specifications were always met independently of the PAPR. For meeting the

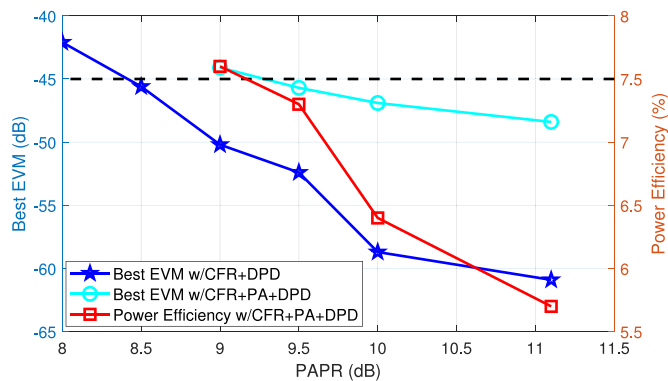


Fig. 16. In-band linearity measured in terms of EVM and power efficiency vs. PAPR reduction.

in-band distortion specifications of $EVM \leq -45$ dB, no more than 1.6 dB of PAPR reduction (corresponding to 9.5 dB of PAPR) was tolerated at the transmitter antenna side, i.e., when considering the RF PA and DPD linearization. As reported in Table II, by reducing the PAPR from 11.1 dB up to 9.5 dB, it is possible to meet the ACPR and EVM specifications, extending the mean output power up to 27.3 dBm and obtaining a power efficiency of 7.3%.

IV. CONCLUSION

A wideband push-pull PA on GaN HEMT technology and with reduced footprint was specifically designed for wired communication applications to deliver around 27 dBm of average output power with reduced even-order distortion in the frequency range of 54–1200 MHz with the maximum power efficiency possible. In order to meet the linearity specifications when operating the PA with wideband signals and high FBW, two DPD behavioral models have been proposed: a RF DPD linearizer based on a BP-GMP behavioral model and a BB I-Q DPD linearizer based on a HD-GMP behavioral model. Both DPD models take into account the harmonic distortion that appears when considering nonlinear amplification of wideband signal with high FBW. From a linearization performance perspective, there are slight differences between the RF and BB DPD approaches, since both can meet the linearity specifications requiring a similar number of coefficients. However, targeting an FPGA implementation, the RF DPD is preferable, because it requires less hardware resources than the BB I-Q DPD. As discussed in [20], handling real-valued signals positively impacts the number of required FPGA multipliers/adders (e.g., Xilinx DSP48E2 blocks) to implement the DPD function in comparison to handling complex-valued signals (i.e., complex multipliers/adders). The FPGA implementation of the proposed RF and BB DPD models will be addressed in future works, where the most challenging part will be meeting the timing closure taking into account the high sampling rates required to handle these signal bandwidths.

In summary, high power efficient amplification of up 7.3% (drain efficiency) was achieved with the custom-designed GaN HEMT push-pull PA when considering a 4×192 MHz composite DOCSIS signal (i.e., around 800 MHz instantaneous bandwidth). The proposed RF and BB DPD strategies (using

less than 400 properly selected coefficients) were combined with the PC CFR technique to meet the out-of-band and stringent in-band linearity requirements with the best possible PA power efficiency at a mean output power ranging from 25 to 27 dBm, in the line of the evolution of CATV amplifiers described in [21]. The linearization performance achieved with the proposed DPD models is expected to be valid in general, regardless of the PA mean output power.

ACKNOWLEDGMENT

The authors would like to thank Xiaoshu Si from Huawei Technologies Co. LTD, Wuhan of China, for his insightful comments and interesting discussions regarding the amplification of DOCSIS signals and the linearity requirements for cable TV applications.

REFERENCES

- [1] S. S. K. C. Bulusu, H. Shaïek, and D. Roviras, "HPA linearization for next generation broadcasting systems with fast convergence-digital predistortion," *IEEE Trans. Broadcast.*, vol. 67, no. 3, pp. 776–790, Sep. 2021.
- [2] J. Wood, *Behavioral Modeling and Linearization of RF Power Amplifiers*. Boston, MA, USA: Artech House Publ., 2014.
- [3] P. L. Gilabert, G. Montoro, D. Vegas, N. Ruiz, and J. A. Garcia, "Digital predistorters go multidimensional: DPD for concurrent multiband envelope tracking and outphasing power amplifiers," *IEEE Microw. Mag.*, vol. 20, no. 5, pp. 50–61, May 2019.
- [4] Z. Liu, X. Hu, W. Wang, and F. M. Ghannouchi, "A joint PAPR reduction and digital predistortion based on real-valued neural networks for OFDM systems," *IEEE Trans. Broadcast.*, vol. 68, no. 1, pp. 223–231, Mar. 2022. [Online]. Available: <https://doi.org/10.1109/TBC.2021.3132158>
- [5] H. Qian, S. Yao, H. Huang, and W. Feng, "A low-complexity digital predistortion algorithm for power amplifier linearization," *IEEE Trans. Broadcast.*, vol. 60, no. 4, pp. 670–678, Dec. 2014.
- [6] P. Pratt and F. Kearney, *Ultrawideband Digital Predistortion (DPD): The Rewards (Power and Performance) and Challenges of Implementation in Cable Distribution Systems*, vol. 51, Analog Dialogue, Wilmington, MA, USA, Jul. 2017.
- [7] P. Pratt, C. Masterson, and J. M. McCormack, "Ultra wide band digital pre-distortion," Patent EP3 166 223 B1, Feb. 2020. [Online]. Available: <https://patents.google.com/patent/EP3166223A2>
- [8] W.-J. Kim, K.-J. Cho, S. P. Stapleton, and J.-H. Kim, "An efficient crest factor reduction technique for wideband applications," *Analog Integr. Circuits Signal Process.*, vol. 51, no. 1, pp. 19–26, Apr. 2007.
- [9] D. López, P. L. Gilabert, G. Montoro, and N. Bartzoudis, "Peak cancellation and digital predistortion of high-order QAM wideband signals for next generation wireless backhaul equipment," in *Proc. Int. Workshop Integr. Nonlinear Microw. Millimetre-Wave Circuits (INMMiC)*, Apr. 2014, pp. 1–3.
- [10] S. H. Han and J. H. Lee, "An overview of peak-to-average power ratio reduction techniques for multicarrier transmission," *IEEE Wireless Commun.*, vol. 12, no. 2, pp. 56–65, Apr. 2005.
- [11] T. Jiang and Y. Wu, "An overview: Peak-to-average power ratio reduction techniques for OFDM signals," *IEEE Trans. Broadcast.*, vol. 54, no. 2, pp. 257–268, Jun. 2008.
- [12] S. Kaur and G. S. Saini, "Review paper on PAPR reduction techniques in OFDM system," *Indian J. Sci. Technol.*, vol. 9, no. 48, pp. 1–6, Jan. 2017.
- [13] V. Volterra, *Theory of Functionals and of Integral and Integro-Differential Equations*. New York, NY, USA: Dover Phoenix Ed., 1959.
- [14] D. Schreurs, M. Odroma, A. A. Goacher, and M. Gadringer, Eds., *RF Power Amplifier Behavioral Modeling*. Cambridge, U.K.: Cambridge Univ. Press, 2008.
- [15] D. R. Morgan, Z. Ma, J. Kim, M. G. Zierdt, and J. Pastalan, "A generalized memory polynomial model for digital predistortion of RF power amplifiers," *IEEE Trans. Signal Process.*, vol. 54, no. 10, pp. 3852–3860, Oct. 2006.

- [16] J. Reina-Tosina, M. Allegue-Martínez, C. Crespo-Cadenas, C. Yu, and S. Cruces, "Behavioral modeling and predistortion of power amplifiers under sparsity hypothesis," *IEEE Trans. Microw. Theory Techn.*, vol. 63, no. 2, pp. 745–753, Feb. 2015.
- [17] Q. A. Pham, D. López-Bueno, G. Montoro, and P. L. Gilibert, "Dynamic selection and update of digital predistorter coefficients for power amplifier linearization," in *Proc. IEEE Topical Conf. RF/Microw. Power Amplifiers Radio Wireless Appl. (PAWR)*, Jan. 2019, pp. 1–4.
- [18] L. Ding, F. Mujica, and Z. Yang, "Digital predistortion using direct learning with reduced bandwidth feedback," in *IEEE MTT-S Int. Microw. Symp. Dig.*, Jun. 2013, pp. 1–3.
- [19] R. N. Braithwaite, "Wide bandwidth adaptive digital predistortion of power amplifiers using reduced order memory correction," in *IEEE MTT-S Int. Microw. Symp. Dig.*, Jun. 2008, pp. 1517–1520.
- [20] W. Li, N. Bartzoudis, J. R. Fernández, D. López-Bueno, G. Montoro, and P. L. Gilibert, "FPGA implementation of a linearization system for wide-band envelope tracking power amplifiers," *IEEE Trans. Microw. Theory Techn.*, early access, Nov. 9, 2022, doi: [10.1109/TMTT.2022.3217842](https://doi.org/10.1109/TMTT.2022.3217842).
- [21] C. Young, "CATV hybrid amplifier modules: Past, present, future," RFMD, Greensboro, NC, USA, RFMD White Paper WP090529, 2009.



Pere L. Gilibert (Senior Member, IEEE) received the M.Sc. degree in telecommunication engineering and the Ph.D. degree (awarded with the Extraordinary Doctoral Prize) from the Universitat Politècnica de Catalunya (UPC) in 2002 and 2008, respectively. He developed his master's thesis at the University of Rome "La Sapienza" with an Erasmus Exchange Grant. He joined the Department of Signal Theory and Communications in 2003. He is an Associate Professor with the Castelldefels School of Telecommunications and Aerospace Engineering.

His research activity is in the field of linearization techniques and digital signal processing solutions for highly efficient transmitter architectures.



José-Ramón Pérez-Cisneros (Member, IEEE) received the Ph.D. degree (*cum laude*) from the University of Zaragoza, Zaragoza, Spain, in 2017. From 2013 to 2017, he was with the Aragon Institute of Engineering Research, University of Zaragoza, being a part of the Mobile Communications Group. From 2017 to 2019, he was a Researcher with the RF and Microwave Group, University of Cantabria, Santander, Spain. From 2019 to 2022, he was a Postdoctoral Researcher with the Microwave Electronics Laboratory, Chalmers University of

Technology, Gothenburg, Sweden. Since 2022, he has been with Ampleon, Toulouse, France. He has authored or coauthored more than 25 publications in international journals and conferences. His current research interests include advanced high-efficiency, linear, and wideband RF power amplifier architectures.



Zhixiong Ren (Member, IEEE) received the Ph.D. degree in microelectronics and solid state electronics from the Huazhong University of Science and Technology, Wuhan, China, in 2016. In 2016, he joined with Huawei as a Research Engineer in access network area from copper/optic wireline access to Wi-Fi wireless access. His main research interests include microwave power amplifier, CMOS power amplifier, phased array RF front-end, CMOS transimpedance, and radio-over-fiber.



in communications systems.

Gabriel Montoro (Member, IEEE) received the M.Sc. degree in telecommunication engineering and the Ph.D. degree from the Universitat Politècnica de Catalunya, Barcelona, Spain, in 1990 and 1996, respectively. He joined the Department of Signal Theory and Communications, Universitat Politècnica de Catalunya in 1991, where he is currently an Associate Professor. His first research works were done on the area of adaptive control, and his current main research interest is in the use of signal processing strategies for power efficiency improvement



María de las Nieves Ruiz Lavín received the M.Sc. and Ph.D. degrees in telecommunications engineering from the University of Cantabria, Santander, Spain, in 2013 and 2017, respectively. She was part of the Department of Communications Engineering, University of Cantabria from 2011 to 2021 involved in high-efficient transmission topologies research projects. Her research was focused on in high-efficiency microwave power amplifiers, rectifiers, oscillators, and dc/dc converters.



José A. García (Member, IEEE) received the B.Sc. degree in telecommunications engineering from Instituto Superior Politécnico "José A. Echeverría" (currently, Universidad Tecnológica de la Habana, CUJAE), Havana, Cuba, in 1988. He received the Ph.D. degree from the Universidad de Cantabria (UC), Santander, Spain, in 2000. From 1988 to 1991, he was a Radio System Engineer with a High-Frequency Communications Center. From 1991 to 1995, he was an Instructor Professor with the Telecommunication Engineering Department,

CUJAE. He worked with Thamat Global Technology Systems as a Radio Design Engineer from 1999 to 2000. From 2000 to 2001, he was a Microwave Design Engineer/Project Manager with TTI Norte. In 2002, he went back to the University of Cantabria as a Senior Research Scientist "Ramón y Cajal," where he is currently an Associate Professor. He was a Postdoctoral Fellow with the Telecommunications Institute, University of Aveiro from 2003 to 2004. During the first half of 2011, he was a Visiting Researcher with the Microwave and RF Research Group, University of Colorado at Boulder. His main research interests include the nonlinear characterization and modeling of GaN HEMTs, as well as the design of efficient RF/microwave power amplifiers, rectifiers, dc/dc power converters, and wireless transmission architectures. He received the Extraordinary Doctoral Prize from UC and an Ex Aequo Prize from Colegio Oficial/Asociación Española de Ingenieros de Telecomunicación for his Ph.D. degree. He was the TPC Chair of EuMIC 2018 (EuMW 2018, Madrid) and served as an Associate Editor for IEEE TRANSACTIONS ON MICROWAVE THEORY AND TECHNIQUES.